CLINICAL GENETICS An International Journal of Genetics, Molecular and Personalized Medicine

Clin Genet 2014: 85: 178–183
Printed in Singapore. All rights reserved

CLINICAL GENETICS
doi: 10.1111/cge.12141

Short Report

Polymicrogyria with dysmorphic basal ganglia? Think tubulin!

Amrom D., Tanyalçin I., Verhelst H., Deconinck N., Brouhard G.J., Décarie J.-C., Vanderhasselt T., Das S., Hamdan F.F., Lissens W., Michaud J.L., Jansen A.C. Polymicrogyria with dysmorphic basal ganglia? Think tubulin!
Clin Genet 2014: 85: 178–183. © John Wiley & Sons A/S. Published by John Wiley & Sons Ltd, 2013

Dominant mutations in *TUBB2B* have been reported in patients with polymicrogyria. We further explore the phenotype associated with mutations in *TUBB2B*. Twenty patients with polymicrogyria (five unilateral) were tested for mutations in *TUBB2B* by Sanger sequencing. We identified two novel *de novo* mutations, c.743C>T (p.Ala248Val) and c.1139G>T (p.Arg380Leu) in exon 4 of *TUBB2B* in three unrelated families. Brain magnetic resonance images showed polymicrogyria involving predominantly the perisylvian regions. In addition, there was a dysmorphic appearance of the basal ganglia, thin corpus callosum, enlargement of the ventricles, thinning of the white matter and hypoplasia of pons and cerebellar vermis. This combination of associated features was absent in all 17 patients with polymicrogyria in whom no mutation was identified. This report underlines that the association of polymicrogyria with thin or absent corpus callosum, dysmorphic basal ganglia, brainstem and vermis hypoplasia is highly likely to result from mutations in *TUBB2B* and provides further insight in how mutations in *TUBB2B* affect protein function.

Conflict of interest

The authors declare no conflict of interest.

D. Amrom[a,b,†], I. Tanyalçin[c,†], H. Verhelst[d], N. Deconinck[e], G.J. Brouhard[f], J.-C. Décarie[g], T. Vanderhasselt[h], S. Das[i], F.F. Hamdan[a], W. Lissens[c,j], J.L. Michaud[a] and A.C. Jansen[k,l]

[a]Centre of Excellence in Neurosciences of Université de Montréal and Sainte-Justine Hospital Research Center, [b]Neurogenetics Unit, Montreal Neurological Hospital, McGill University, Montreal, Canada, [c]Centre for Medical Genetics, UZ Brussel, Brussels, Belgium, [d]Department of Pediatric Neurology, Ghent University Hospital, Ghent, Belgium, [e]Department of Neurology, Hôpital Universitaire des Enfants Reine Fabiola, Université Libre de Bruxelles, Brussels, Belgium , [f]Department of Biology, McGill University , [g]Department of Radiology, Sainte-Justine Hospital, Montreal, Canada, [h]Department of Radiology, UZ Brussel, Brussels, Belgium, [i]Department of Human Genetics, University of Chicago, Chicago, IL, USA, [j]Research Group Reproduction and Genetics, Vrije Universiteit Brussel, [k]Pediatric Neurology Unit, Department of Pediatrics, Universitair Ziekenhuis Brussel, and [l]Department of Public Health, Vrije Universiteit Brussel, Brussels, Belgium

[†]These authors contributed equally to this work.

Key words: basal ganglia – corpus callosum – malformations of cortical development – polymicrogyria – TUBB2B

Corresponding author: Dina Amrom, MD, Neurogenetics Unit, Room 127, Montreal Neurological Hospital and Institute, 3801 University Street, Montreal, Quebec H3A 2B4, Canada.
Tel.: +1 5143988529;
fax: +1 5143981276;
e-mail: dina.amrom@mcgill.ca

Received 23 December 2012, revised and accepted for publication 11 March 2013

Genes encoding for tubulin proteins have been identified as a cause for malformations of cortical development. The high sequence similarity between tubulin paralogs has prompted sequencing of candidate genes such as *TUBA1A*, *TUBA8*, *TUBB2B*, *TUBB3* and *TUBB5* in search of pathogenic mutations, and several missense and nonsense mutations have been reported in these genes. However, both similarities and distinctive effects of tubulin mutations have been observed at the level of the cortical phenotype (1). *TUBB2B* encodes for the beta subunit of the tubulin α/β heterodimer, which is incorporated into growing microtubules and is ubiquitously expressed in migrating, dividing and differentiating neurons (2, 3). To date, 14 mutations, 13 occurring *de novo* and 1 with dominant inheritance have been reported, resulting in focal to more diffuse, mostly asymmetric, polymicrogyria in all patients, except in one who had a diffuse cortical malformation compatible with lissencephaly (4–8). We report two unrelated patients harboring the same heterozygous *de novo* p.Ala248Val mutation and a third patient with a *de novo* p.Arg380Leu mutation in *TUBB2*, contributing to a further delineation of the *TUBB2B* associated phenotype, and provide insight on the impact of both mutations on tubulin function.

Materials and methods

Mutation analysis

Patient 1 was tested for mutations in *TUBA1A* and *TUBB2B* (RefSeq NM_178012.4) at the Department of Human Genetics, University of Chicago, United States, as reported by Jaglin et al. (4). All other patients were tested at the Center for Medical Genetics, UZ Brussel, Belgium, after mutations in *TUBA1A* had been ruled out. For the patients in whom a mutation was identified, targeted mutation analysis was performed in the parents to verify the *de novo* character of the mutation. The study protocol has been approved by the Research Ethics Board of the UZ Brussel and the Research Ethics Boards of the Sainte-Justine Hospital.

Protein structural modeling

Dynein on microtubules (Fig. 2b) have been generated by superimposing the dynein stalk domain of 3J1T (9) with 3VKH (10) and the tubulin dimers with 1TUB [100% sequence identity with human TUBB2B (11)]. Labeling of the mutation (Fig. 2d) was performed on 1TUB. The mutated model (Fig. 2e) was obtained by submitting the raw Tubb2b sequence (Refseq:NP_821080; Uniprot:Q9BVA1) to the automated I-TASSER server (http://zhanglab.ccmb.med.umich.edu/) (12–14). The resulting model was compared with two additional Tubb2b models from SWISS-MODEL Repository (http://swissmodel.expasy.org/repository/) based on 3HKE and 4DRX for validation. Parceling of the Tubb2b surface was generated by superimposing human Tubb2b from SWISS-MODEL Repository (based on 3HKE), 1TUB, 3VKH, 31JT and 4FFB (15). Molecular surfaces were contoured based on the electrostatic potentials with coulomb computation method and taking into account atomic partial charges. All models are accessible through the Protein Data Bank website (http://www.rcsb.org/). All renderings and modifications were performed on DeepView–Swiss-PdbViewer (http://www.expasy.org/spdbv/) (16–18). Images were post-processed with POV-Ray v3.6 (http://www.povray.org).

Energy minimization and model refinement

Three models (two from SWISS-MODEL repository and one from I-TASSER) were loaded on Swiss-PDB viewer and manually mutated. For energy minimization, two cycles of steepest descent consisting of 50 steps each and one cycle of conjugate gradient consisting of 200 steps with a minimum ΔE of 0.01 kJ/mol were performed together with a harmonic constraint of 100 kJ/mol. The resulting models were further refined using the ModRefiner (http://zhanglab.ccmb.med.umich.edu/ModRefiner/, Job IDs 2292, 2731, 2732, 2733, 2734, 2735, 2736, 2748, 2749, 2750, 2882) (19). Before comparison, the same procedure was performed on the unaltered wild-type models to avoid bias.

Results

Clinical findings

All patients were born to non-consanguineous unrelated parents. Presenting features included developmental delay, focal seizures or epileptic spasms (Table 1). All patients had severe psychomotor delay. All children could understand simple commands and patients 1 and 2 could express single words. Attention span was very short in all. Bilateral convergent strabismus was present in patients 2 and 3. Head circumference varied from just below P3 to P25. Brain magnetic resonance imaging (Fig. 1) showed asymmetric polymicrogyria of various localisation and extent, involving predominantly the perisylvian regions. All patients had abnormal basal ganglia with dysgenesis of the anterior limb of the internal capsule resulting in a fusion of the caudate nucleus and putamen, as well as a dysmorphic appearance of the striatum. All had enlarged lateral ventricles with a hooked aspect of the anterior horn, thinning of the white matter, thin corpus callosum and hypoplasia of brainstem and cerebellar vermis. The optic chiasma was hypoplastic in patient 1.

Table 1. Summary of clinical and imaging features

Patient	1	2	3
Mutation	p.R380L	p.A248V	p.A246V
Clinical findings			
Age at examination/sex	4.5 years/F	6.5 years/M	4 years/M
Origin	French-Canadian	Turkish	Belgian
Presenting symptoms/age	Developmental delay/10 months	Developmental delay, epilepsy/2.5 years	Epileptic spasms/5.5 months
Motor development	Walked independently at 3 years	Walked independently, poor balance	Walked with bilateral support
Cognition	Severe cognitive impairment	Severe cognitive impairment	Severe cognitive impairment
Receptive speech	Understanding of simple commands	Understanding of simple commands	Understanding of simple commands
Expressive speech	Single words	Single words	No words
Epilepsy	Absent	Focal nocturnal seizures	Infantile spasms
Oculomotor nerves	Normal	Bilateral convergent strabismus	Bilateral convergent strabismus
Others	Mild facial dysmorphism	–	Mild facial dysmorphism
Brain MRI			
Polymicrogyria	Asymmetric perisylvian, parietal L>R	Asymmetric R perislyvian region	Asymmetric R fronto-parietal and L frontal lobes
Corpus callosum	Thin	Thin	Thin
Basal ganglia	Dysmorphic	Dysmorphic	Dysmorphic
Internal capsule	Dysgenesis of the anterior limb	Dysgenesis of the anterior limb	Dysgenesis of the anterior limb
Ventricles	Dilated, hooked anterior horn	Dilated, hooked anterior horn	Dilated, hooked anterior horn
White matter	Thinned	Thinned	Thinned
Optic nerves	Optic nerve hypoplasia	Normal	Normal
Brainstem	Hypoplasia	Hypoplasia	Hypoplasia
Cerebellum	Disorganized vermis	Vermis hypoplasia	Vermis hypoplasia
Other features	–	–	Bilateral frontal multifocal hyperintense signals on FLAIR sequences

F, female; FLAIR, fluid attenuated inversion recovery; L, left; M, male; MRI, magnetic resonance imaging; R, right.

Sequencing analysis of *TUBB2B* revealed two novel *de novo* heterozygous missense mutations in exon 4: c.1139G>T (p.Arg380Leu) in patient 1 and c.743C>T (p.Ala248Val) in patients 2 and 3 (Fig. 2a).

Location of the affected residues in the protein

In the p.Ala248Val variant, the residue constitutes the first alanine of the 43 amino acid long invariant sequence 'TMSG . . . QLN*A* . . . APLT' and in the p.Arg380Leu variant, the residue is the last arginine residue of the 16 amino acid long 'ATFI . . . LFK*R*' section of exon 4 in *TUBB2B*, which is well conserved across vertebrates, even partially down to *Drosophila melanogaster* and *Caenorhabditis elegans*. According to the refined and energy minimized human TUBB2B models, the conserved alanine residue is also located approximately 6 Å away from the non-exchangeable GTP of the preceding α-tubulin monomer and comprises part of a coil structure between the two α-helix structures encompassing the invariant sequence (Fig. 2e) and the conserved arginine residue is located about 13 Å from the exchangeable GDP molecule of Tubb2b (Fig. 2e).

Discussion

Mutations in genes belonging to the tubulin family have been reported in a broad spectrum of malformations of cortical development ranging from polymicrogyria to malformations in the agyria/pachygyria spectrum, with or without congenital fibrosis of the extraocular muscles or optic nerve hypoplasia (1). We report two novel mutations in *TUBB2B* associated with a complex disorder of brain development, associating polymicrogyria with dysmorphic basal ganglia, thin corpus callosum and hypoplasia of brainstem and cerebellar vermis in three unrelated families. The associated brain malformations were absent in all 17 patients with polymicrogyria in whom no mutation in *TUBB2B* was identified. The changes in the basal ganglia result in a hooked aspect of the anterior horn of the lateral ventricles (Fig. 1b,e,h), which is an easy sign for clinicians to check on imaging and can

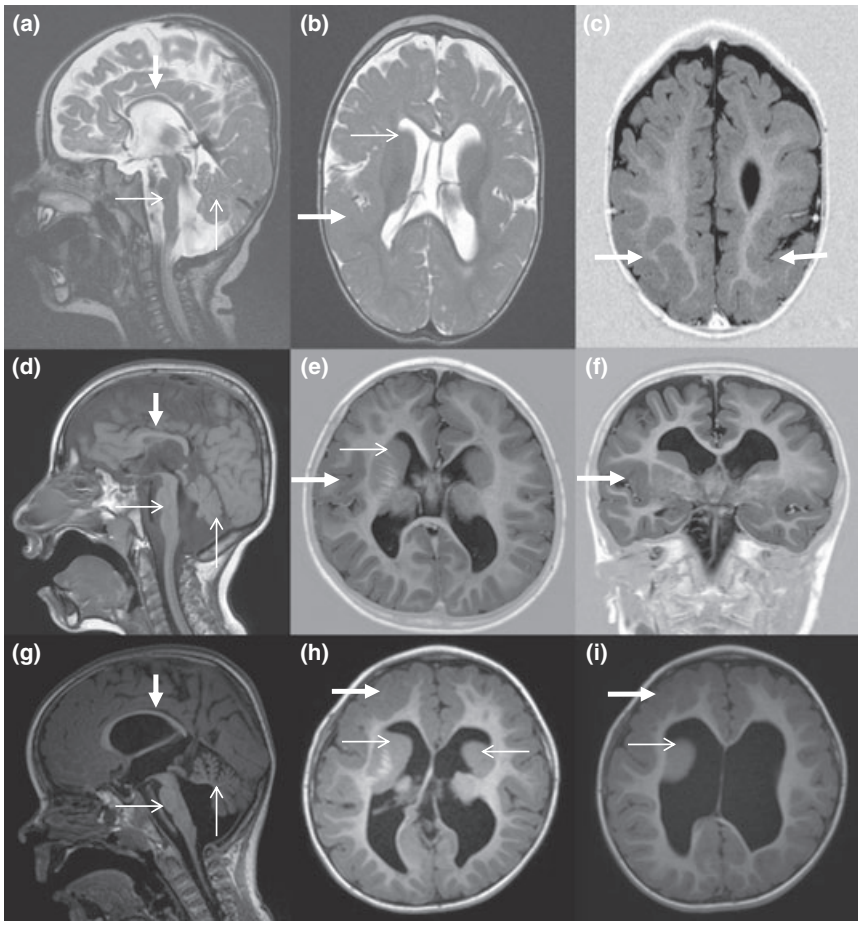

Fig. 1. Magnetic resonance imaging of individuals with *TUBB2B* mutations: patient 1 (**a–c**), patient 2 (**d–f**), patient 3 (**g–i**). Sagittal images show thin corpus callosum (thick arrow) and hypoplasia of pons and cerebellum (thin arrows) (**a**, **d**, **g**). Axial images show an abnormal shape of the basal ganglia with dysgenesis of the anterior limb of the capsula interna resulting in a hooked aspect of the lateral ventricles (thin arrows) (**b**, **e**, **h**) and areas of polymicrogyria (thick arrows) over the posterior regions (**b**, **c**), in the right perisylvian area (**e**) and in the right frontoparietal regions (**h**, **i**). Axial and coronal images show enlarged ventricles and thinning of the white matter (**b**, **c**, **e**, **f**, **h**, **i**).

assist with the orientation of molecular genetic testing. Although basal ganglia are not always abnormal, the combination of dysmorphic basal ganglia with polymicrogyria is highly suggestive of mutations in *TUBB2B*, and, to a lesser extent, *TUBA1A* (20). Dysmorphic basal ganglia with agyria/pachygyria most frequently result from mutations in *TUBA1A*, but can also be encountered with mutations in *TUBB2B* (8). As the α- and β-tubulins share 40% amino acid sequence identity (http://www.ebi.ac.uk/Tools/msa/clustalo/) (21) and form an α/β tubulin heterodimer, it is conceivable that mutations in *TUBB2B* can result in a spectrum of brain malformations similar to that caused by mutations in *TUBA1A* and vice versa. The association of a thin corpus callosum, hypoplasia of pons and cerebellum can also be seen in association with bilateral frontoparietal polymicrogyria caused by mutations in the *GPR56* gene. Of note is the occurrence of myelination defects in the latter condition (22). Cederquist et al. reported asymmetric white matter tract abnormalities in three patients from a single family with a p.E421K *TUBB2B* mutation (7). Polymicrogyria associated with optic nerve hypoplasia as seen in patient 1 has been reported in association with mutations in *TUBA8* (23) and *TUBA1A* (20).

The independent occurrence of the c.743C>T (p.Ala248Val) mutation in two families of different ethnic origin, as well as the predicted effect of both the c743C>T (p.Ala248Val) and c.1139G>T (p.Arg380Leu) mutations on protein function by SIFT (PMID: 22689647) and MUTPRED (PMID: 19734154) mutation prediction algorithms further consolidates the pathogenic nature of these mutations.

Figure 2c shows the parceling out of the TUBB2B protein surface into functional areas showing the distribution of vital residues on the protein's surface area, signifying the state of 'near perfection', these proteins have achieved through the course of evolution.

Ala248 is situated in an interface where the α-tubulin facade has relatively more negative electrostatic potential compared to the β-tubulin facade. Although valine has no net charge, *in silico* analysis suggests that substitution of alanine by valine results in a gain of positive electrostatic potential on the β-tubulin facade. On the other hand, Arg380 is located on the opposite side, close to the exchangeable GDP molecule and *in*

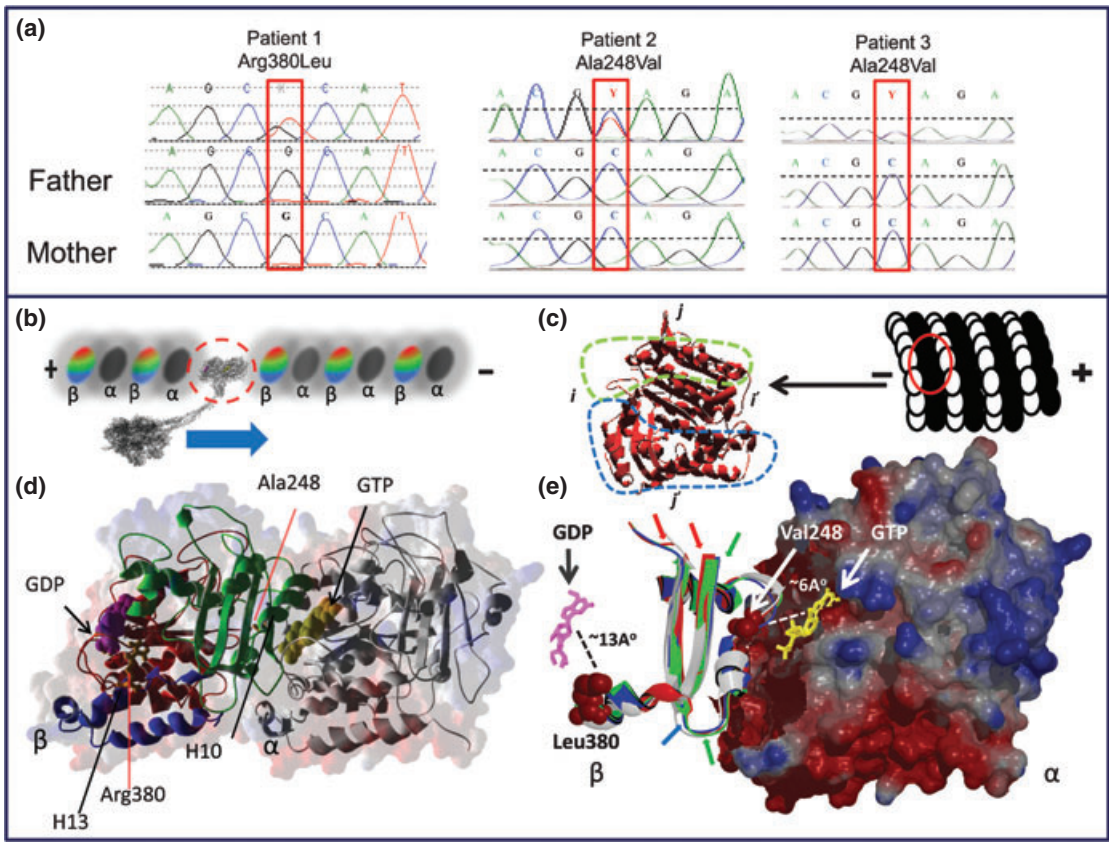

Fig. 2. (**a**) Electropherogram. Sequencing analysis for the *de novo* c.1139G>T (p.Arg380Leu) and the c.743C>T (p.Ala248Val) mutation. Patients 2 and 3 are carriers of the same mutation. Dashed lines designate the same level of intensity. (**b**) Cartoon representation of a dynein molecule attached to a microtubule. Tuba1a proteins are depicted in gray spheres whereas TUBB2B in colored. Blue arrow denotes the direction of dynein's propagation. (**c**) Surface parceling of TUBB2B based on function. Facades *i* and *i′* are involved in longitudinal interactions whereas *j* and *j′* are involved in lateral interactions. The top face of Tubb2b (SWISS-MODEL Repository based on 3HKE) is involved in heterodimer formation by interacting with a microtubule polymerase Stu2 (homologous to Xmap215 in *X. tropicalis* and Ckap5 in *H. Sapiens*) and dynein binding (congruence achieved by superimposing the Tubb2b model with 3J1T and 3VKH). (**d**) Three-dimensional ribbon model of a tubulin heterodimer (1TUB). The N-terminal region, intermediate zone and the C-terminal region of TUBB2B (residues 1–205, 206–381 and 382–445) is colored in red, green and blue, respectively (5) The conserved alanine residue (orange) is located behind the H10 of Tubb2b whereas the conserved arginine residue (orange) is adjacent to H13. The guanosine molecules are depicted with the Van Der Waals surface (magenta, exchangeable GDP; yellow non-exchangeable GTP). (**e**) Site of mutation. Only the 43 and the 16 amino acid long partially conserved regions around the mutated residues Val248 and Leu380 of Tubb2b with molecular surface of Tuba1a (1TUB) is shown for clarity (models based on 3HKE, 4DRX and I-TASSER depicted in red, green and blue, respectively). Gray ribbon structures represent the native state of the protein whereas the colored ribbon structures represent the conformation post-mutation. The molecular surface is contoured according to electrostatic charge, where gradients of red and blue colors depict areas of negativity and positivity, respectively. The valine and the leucine residues are approximately situated 6 Å away from the non-exchangeable GTP of tuba1a and 13 Å away from the exchangeable GDP of Tubb2b, respectively. Both substitutions also result in a slight change in electrostatic forces (data not shown).

silico analysis suggests that its substitution by leucine results in a gain of negative electrostatic potential. As tubulins are incorporated into growing microtubules as heterodimers mediated by proteins with TOG domains (24), a minor change in the electrostatic potentials may impede the overall turnover of heterodimers. It is noteworthy that electrostatic interactions may also account for dynein–tubulin interactions. This renders the possibility of an 'avalanche effect' at the event of a slight change in the electrostatic potential of tubulins triggered by mutations, concomitantly impairing both the turnover of heterodimers and motor protein interactions. Interestingly, both Ala248Val and Arg380Leu mutations result in an overall root mean square deviation (RMSD) change that is lower than the RMSD change where only residues that are in contact with the GDP molecule are taken into account (Fig. S1). These residues are highly conserved ever since the divergence of tubulins from their ancestral FtsZ counterpart (25) and it may be that the functional acquisitions throughout the evolution were gradually evolved if and only if they do not impinge on the properties of these highly conserved residues. This brings forth the possibility of an 'allosteric effect' for *TUBB2B* mutations, where mutations are able to grossly alter conserved regions even though physically far away from them. Nonetheless, although *in silico* data provide guidelines on which prospective functional studies can be based upon, they should always be handled with caution.

Tubulin proteins associate with various chaperone proteins prior to heterodimer formation and therefore mutations may be able to stifle microtubule dynamics

by either diminishing their formation or generating dysfunctional oligomers (4). RNAi and mutagenesis studies have shown that a low concentration of functional tubulin monomers and polymerization or tubulin-specific chaperones interaction deficient mutants virtually converge to the same phenotypic outcome due to dynamic instability of microtubules, resulting in a phenotypic overlap (4).

This article corroborates the phenotype associated with mutations in *TUBB2B* and illustrates how imaging can assist with the selection of patients for mutation analysis of this gene. Although next-generation sequencing techniques might facilitate the identification of a causative gene mutation in some patients, a significant number of patients will not have access to these facilities in the near future and clinical or imaging clues assisting with the orientation of targeted gene sequencing might still be helpful.

Supporting Information

The following Supporting information is available for this article:

Figure S1. (**a**) Conserved residues. The conserved residues of Tubb2b that are in close proximity to GDP are colored green/red. C^{α} backbone, gray; GDP, magenta with Van der Waals surface, red marks residues in contact with GDP. (**b**) Partial peptide sequence alignment of human Tubb2b (NP_821080) with FtsZ protein from *Methanocaldococcus jannaschii* (Q57816), *Staphylococcus aureus* (P0A031) and *Escherichia coli* (P0A9A6). Numbers pertain to human Tubb2b sequence. Residues that are in contact with the GDP molecule are colored in red. (**c**) Box plot of root mean square deviation (RMSD) values for mutated *vs* wild-type (1TUB, B chain) protein. Three proposed mutated forms of human Tubb2b (two models from SWISS-MODEL Repository, based on 3HKE and 4DRX, one model from I-TASSER, Job ID S109651) have been compared in means of overall RMSD (>300 residues involved), RMSD of the conserved residues depicted in (**b**) and the geometric mean of RMSD of two random patches upstream and downstream of the conserved sequence (Arg251-Phe260, Met299-Asp304 and Asn14-Val23, Arg62-Asp67) to avoid bias.

Additional Supporting information may be found in the online version of this article.

Acknowledgements

The authors acknowledge the families for their collaboration. D. A. has been funded by a grant from RMGA (Réseau de Médecine génétique appliquée). I. T. is funded by a grant from UZOR (UZ Brussel Onderzoeksraad). A. J. received support from the Scientific Fund Willy Gepts.

References

1. Tischfield MA, Cederquist GY, Gupta ML Jr, Engle EC. Phenotypic spectrum of the tubulin-related disorders and functional implications of disease-causing mutations. Curr Opin Genet Dev 2011: 21: 286–294.
2. Higginbotham HR, Gleeson JG. The centrosome in neuronal development. Trends Neurosci 2007: 30: 276–283.
3. Heng JI, Chariot A, Nguyen L. Molecular layers underlying cytoskeletal remodelling during cortical development. Trends Neurosci 2009: 33: 38–47.
4. Jaglin XH, Poirier K, Saillour Y et al. Mutations in the beta-tubulin gene TUBB2B result in asymmetrical polymicrogyria. Nat Genet 2009: 41: 746–752.
5. Guerrini R, Mei D, Cordelli DM et al. Symmetric polymicrogyria and pachygyria associated with TUBB2B gene mutations. Eur J Hum Genet 2012: 20: 995–998.
6. Romaniello R, Tonelli A, Arrigoni F et al. A novel mutation in the beta-tubulin gene TUBB2B associated with complex malformation of cortical development and deficits in axonal guidance. Dev Med Child Neurol 2012: 54: 765–769.
7. Cederquist GY, Luchniak A, Tischfield MA et al. An inherited TUBB2B mutation alters a kinesin-binding site and causes polymicrogyria, CFEOM and axon dysinnervation. Hum Mol Genet 2012: 21: 5484–5499.
8. Cushion TD, Dobyns WB, Mullins JG et al. Overlapping cortical malformations and mutations in TUBB2B and TUBA1A. Brain 2013: 136: 536–548.
9. Redwine WB, Hernandez-Lopez R, Zou S et al. Structural basis for microtubule binding and release by dynein. Science 2012: 337: 1532–1536.
10. Kon T, Oyama T, Shimo-Kon R et al. The 2.8 A crystal structure of the dynein motor domain. Nature 2012: 484: 345–350.
11. Nogales E, Wolf SG, Downing KH. Structure of the alpha beta tubulin dimer by electron crystallography. Nature 1998: 391: 199–203.
12. Zhang Y. I-TASSER server for protein 3D structure prediction. BMC Bioinformatics 2008: 9: 40.
13. Roy A, Kucukural A, Zhang Y. I-TASSER: a unified platform for automated protein structure and function prediction. Nat Protoc 2010: 5: 725–738.
14. Roy A, Yang J, Zhang Y. COFACTOR: an accurate comparative algorithm for structure-based protein function annotation. Nucleic Acids Res 2012: 40: W471–W477.
15. Ayaz P, Ye X, Huddleston P et al. A TOG:alphabeta-tubulin complex structure reveals conformation-based mechanisms for a microtubule polymerase. Science 2012: 337: 857–860.
16. Peitsch MC. Protein modeling by E-mail. Nat Biotechnol 1995: 13: 658–660.
17. Kiefer F, Arnold K, Kunzli M et al. The SWISS-MODEL Repository and associated resources. Nucleic Acids Res 2009: 37: D387–D392.
18. Arnold K, Bordoli L, Kopp J et al. The SWISS-MODEL workspace: a web-based environment for protein structure homology modelling. Bioinformatics 2006: 22: 195–201.
19. Xu D, Zhang Y. Improving the physical realism and structural accuracy of protein models by a two-step atomic-level energy minimization. Biophys J 2011: 101: 2525–2534.
20. Jansen AC, Oostra A, Desprechins B et al. TUBA1A mutations: from isolated lissencephaly to familial polymicrogyria. Neurology 2011: 76: 988–992.
21. Sievers F, Wilm A, Dineen D et al. Fast, scalable generation of high-quality protein multiple sequence alignments using Clustal Omega. Mol Syst Biol 2011: 7: 539.
22. Piao X, Chang BS, Bodell A et al. Genotype-phenotype analysis of human frontoparietal polymicrogyria syndromes. Ann Neurol 2005: 58: 680–687.
23. Abdollahi MR, Morrison E, Sirey T et al. Mutation of the variant alpha-tubulin TUBA8 results in polymicrogyria with optic nerve hypoplasia. Am J Hum Genet 2009: 85: 737–744.
24. Al-Bassam J, Chang F. Regulation of microtubule dynamics by TOG-domain proteins XMAP215/Dis1 and CLASP. Trends Cell Biol 2011: 21: 604–614.
25. Lowe J, Amos LA. Crystal structure of the bacterial cell-division protein FtsZ. Nature 1998: 391: 203–206.